

PCCP

Accepted Manuscript



This is an *Accepted Manuscript*, which has been through the Royal Society of Chemistry peer review process and has been accepted for publication.

Accepted Manuscripts are published online shortly after acceptance, before technical editing, formatting and proof reading. Using this free service, authors can make their results available to the community, in citable form, before we publish the edited article. We will replace this *Accepted Manuscript* with the edited and formatted *Advance Article* as soon as it is available.

You can find more information about *Accepted Manuscripts* in the [Information for Authors](#).

Please note that technical editing may introduce minor changes to the text and/or graphics, which may alter content. The journal's standard [Terms & Conditions](#) and the [Ethical guidelines](#) still apply. In no event shall the Royal Society of Chemistry be held responsible for any errors or omissions in this *Accepted Manuscript* or any consequences arising from the use of any information it contains.



Polycyclic Aromatic Hydrocarbon (PAH) Formation from Benzyl Radicals: A Reaction Kinetics Study

Sourab Sinha^{a,b} and Abhijeet Raj^{a,*}

Received 00th January 20xx,
Accepted 00th January 20xx

DOI: 10.1039/x0xx00000x

www.rsc.org/

The role of resonantly stabilized radicals such as propargyl, cyclopentadienyl and benzyl in the formation of aromatic hydrocarbons such as benzene and naphthalene in the high temperature environments has been long known. In this work, the possibility of benzyl recombination to form three-ring aromatics, phenanthrene and anthracene, is explored. A reaction mechanism for it is developed, where reaction energetics are calculated using density functional theory (B3LYP functional with 6-311++G(d,p) basis set) and CBS-QB3, while temperature-dependent reaction kinetics are evaluated using transition state theory. The mechanism begins with barrierless formation of bibenzyl from two benzyl radicals with the release of 283.2 kJ/mol of reaction energy. The further reactions involve H-abstraction by H atom, H-desorption, H-migration, and ring closure to gain aromaticity. Through mechanism and rate of production analyses, the important reactions leading to phenanthrene and anthracene formation are determined. Phenanthrene is found to be the major product at high temperatures. Premixed laminar flame simulations are carried out by including the proposed reactions for phenanthrene formation from benzyl and compared to experimentally observed species profiles to understand their effects on species concentrations.

1. INTRODUCTION:

Soot particles and polycyclic aromatic hydrocarbons are present in the exhaust gas from combustion devices such as engines and furnaces, and are a result of incomplete combustion of fuels. While the harmful effects of soot particles on human health such as respiratory and cardiac problems and on the environment such as global warming and darkening of polar icecaps are known for a long time, their formation path is less understood^{1,2}. Several studies on the characterization of soot particles highlight that they are mainly composed of polycyclic aromatic hydrocarbons (PAHs) with some aliphatic chains that are held together by van der Waals force of attraction³. Thus, to understand the pathways for the formation and growth of soot particles, it is important to determine the pathways for the growth of PAHs in combustion environments.

Several mechanisms have been proposed in the literature for the formation and growth of PAHs^{2,4-9}. The most popular among them is hydrogen-abstraction-acetylene-addition (HACA) mechanism. It involves H-abstraction from a PAH by another H atom to create a radical site. This is followed by C₂H₂ addition to the radical site and ring closure. Several recent studies have highlighted that HACA mechanism under-predicts the concentration profiles of PAHs in hydrocarbon flames¹⁰⁻¹³. Moreover, in our previous study¹⁰, it was shown that HACA mechanism is also unable to predict the synergistic effect of PAHs in the flames of mixture fuels that demonstrates enhanced formation of PAHs for mixture fuels as compared to respective pure fuels due to chemical crosslinking between the species generated from different fuel components. Therefore, other reactions must be contributing to PAH formation and growth. In this direction, the growth of PAHs by several radical species such as CH₃¹⁴ and C₆H₅¹⁵ have been proposed in the past due to their high reactivity, but they may be

^a Department of Chemical Engineering, The Petroleum Institute, Abu Dhabi, UAE.

^b Department of Chemistry, Arya Vidyapeeth College, Guwahati, India

* Email: abgupta@pi.ac.ae

ARTICLE

Physical Chemistry Chemical Physics

mainly effective in the flames where those radicals are in abundance (e.g. CH₄, C₃H₈ and C₆H₆ flames).

In sooting combustion environments, resonantly stabilized radicals (RSRs) are present in abundance due to their higher stability than other radicals through the delocalization of the free electron^{4, 8, 16, 17}. Some common hydrocarbon RSRs are propargyl (C₃H₃), allyl (C₃H₅) cyclopentadienyl (C₅H₅), benzyl (C₆H₅CH₂) and indenyl (C₉H₇). The recombination reactions of some of these RSRs to form aromatic species are well known. For example, C₃H₃ recombination is the most important reaction leading to benzene formation in combustion environments, whose kinetics and mechanism are well established¹⁸⁻²¹. Similarly, C₅H₅ recombination leads to the formation of naphthalene²². In²³, Lu et al. have extended the mechanism of naphthalene formation from C₅H₅ by studying indenyl recombination to form three C₁₈H₁₂ isomers (chrysene, benzo[c]phenanthrene and benz[a]anthracene).

The RSRs can also undergo combination reactions with other RSRs and stable species to contribute to molecular-weight growth chemistry in combustion²³⁻³¹. In^{10, 11}, the reactions involving different RSRs that are responsible for PAH formation and growth are listed. In¹², the reaction mechanism through which C₃H₃ could lead to the growth of PAHs was studied, where the growth of naphthalene to form pyrene was shown to take place through the subsequent additions of C₃H₃ radicals. Colket et al.³² and Marinov et al.³³ have independently established the mechanism of naphthalene formation through the combination of benzyl and propargyl (C₆H₅CH₂ + C₃H₃ → naphthalene + 2H), that have been shown in^{10, 11} to be important reactions for naphthalene formation.

Benzyl is considered to be a potent RSR with its resonance structure relatively parallel to the allyl radicals²⁷. It is readily formed in flames through H abstraction (by H or OH) from toluene

³⁴, or from the combination of small hydrocarbon molecules such as 1-methylallyl (C₄H₅) and C₃H₃ through the reaction: C₄H₅ + C₃H₃ → C₆H₅CH₂ + H^{9, 35}. While benzyl can react with other radicals to form PAHs (as shown above), it can also undergo recombination reaction to form phenanthrene (C₁₄H₁₀): 2C₆H₅CH₂ → C₁₄H₁₀ + 2H₂³⁶. A brief mechanism for this overall reaction was proposed in³⁶, as shown below, but the rates for the elementary reactions involved in it were either guessed or were taken from experimental investigation on benzyl recombination to form bibenzyl (C₁₄H₁₄).

Reaction	Source of Rate constant
C ₆ H ₅ CH ₂ + C ₆ H ₅ CH ₂ → C ₁₄ H ₁₄	³⁷
C ₁₄ H ₁₄ → C ₆ H ₅ CH ₂ + C ₆ H ₅ CH ₂	Estimated
C ₁₄ H ₁₄ + H → C ₁₄ H ₁₂ + H ₂ + H	Estimated
C ₁₄ H ₁₄ ↔ C ₁₄ H ₁₂ + H ₂	Assumed same as C ₄ H ₆ = C ₄ H ₄ + H ₂
C ₁₄ H ₁₂ ↔ C ₁₄ H ₁₀ + H ₂	Assumed same as C ₄ H ₆ = C ₄ H ₄ + H ₂

In our previous studies involving flame simulations to study PAH growth¹⁰, this pathway was found to be significantly contributing to phenanthrene formation. However, as mentioned above, since most of the rate constants for the involved reactions are not from any theoretical or experimental investigations, they are less reliable. Moreover, no detailed mechanistic study exists in the literature on benzyl recombination to explore favourable pathways for phenanthrene formation.

This work presents a study on the development of a reaction mechanism for the formation of phenanthrene from the combination of two benzyl radicals. The possible pathways for the decomposition of bibenzyl that results from this addition reaction will be explored. Quantum chemical calculations will be performed to determine the energetics and the molecular parameters of various intermediate species. The rate constants of the elementary reactions will be evaluated using transition state theory, and validated, wherever possible, with experimental data. Through rate of production analysis, the important reactions for phenanthrene

formation will be determined. The new reactions will also be included in a literature-based mechanism for toluene oxidation, and their effects on the concentrations of aromatic species will be reported.

2. COMPUTATIONAL DETAILS

The ground state molecular structures of the stable intermediate species as well as the transition states were found using Density Functional Theory (DFT) with Becke three-parameter exchange and Lee, Yang and Parr correlation (B3LYP) functional with 6-311++G(d,p) basis set. For large molecules such as aromatic hydrocarbons, DFT is considered to be a standard choice, as it is computationally less expensive than higher levels of theory, and has been validated and used for aromatic hydrocarbons in previous studies^{2, 10, 38-40}. For all the species and the transition states, CBS-QB3 calculations were also conducted to find the differences in reaction and activation energies of the elementary reactions with the change in the level of theory. CBS-QB3 was chosen for this study as it has been shown in^{41, 42} to provide a good accuracy in computed energies in a reasonable computational time. However, as discussed in⁴³, to obtain a higher accuracy in the calculated parameters, the higher levels of theory should be considered. The molecular structures were optimized with different spin multiplicities to identify the multiplicity with a minimum energy, reasonable geometry (i.e. molecular structures correctly representing the reactions being studied), and low spin contamination. Spin contamination affects the energy, geometry and calculated spin density of the molecules. The expectation value of the spin operator \widehat{S}^2 , $\langle S^2 \rangle$ gives a measure of spin contamination. In the case of no spin contamination, $\langle S^2 \rangle$ is equal to $s(s+1)$, where s is half the number of unpaired electrons. If the

difference between $\langle S^2 \rangle$ and $s(s+1)$ is less than 10%, spin contamination can be considered to be low³⁹. The majority of the intermediate species and transition states found in this study were either closed-shell singlets or open-shell doublets, and their spin multiplicities are provided in the supplementary material. All the calculations were performed using Gaussian 09 software⁴⁴.

The rate constants for the reactions involved in the proposed processes were evaluated using transition state theory. The partition functions for the transition states and reactants were calculated at a range of temperatures (300–3000 K) using the vibrational frequencies, moments of inertia, mass and electronic multiplicity, all of which are given by the quantum calculations. Further details are provided in³⁴. A linear least-square fitting algorithm was used to fit the modified Arrhenius expression ($k = AT^n e^{(-E/RT)}$) to the data points of the rate constants in order to obtain the kinetic parameters of the frequency factor A , the temperature exponent n and the activation energy E . To assess the role of quantum tunnelling, in the literature, there are four efficient methods to evaluate the tunnelling correction factor (or, transmission constant): Wigner correction, Eckart correction, zero-curvature tunnelling correction, and small curvature tunnelling correction. At temperatures above 500 K, the correction factors from all the methods converge to similar values^{45, 46}. In this paper, Wigner method was employed to obtain the tunnelling correction factors for all the elementary reactions³⁴.

3. RESULTS AND DISCUSSION:

Figure 1 presents the mechanism through which two benzyl radicals can combine together to form three-ring aromatics, phenanthrene and anthracene. In total, 63 reactions involving 46 species were found. The figure also provides the numbers assigned to the

ARTICLE

Physical Chemistry Chemical Physics

intermediate species (IS) and the transition states (TS) that will be used to identify them. For simplicity, the reaction mechanism has been divided into four pathways. Each pathway would describe a possible channel for the decomposition of bibenzyl (the adduct formed through benzyl recombination) either through the loss of one H atom to create a radical site or through the simultaneous loss of two H atoms from the same or different C atoms to form H₂. The energy values used in the mechanism discussion below are those obtained from CBS-QB3, while the potential energy diagrams provide energies obtained from both CBS-QB3 and B3LYP/6-311++G(d,p).

Figure 2 shows the numbering of carbon atoms on phenanthrene that would help in describing the reaction mechanism.

3.1. Pathway 1

Figure 3 provides the potential energy diagram for benzyl recombination and the further molecular rearrangements to form phenanthrene through Pathway 1. The self-addition of benzyl radicals, leading to bibenzyl (IS1) formation, is a barrierless and highly exothermic reaction with a reaction energy of 283.2 kJ/mol. In ²⁷, Akira *et al.* performed a similar study, where two resonantly stabilized radicals (benzyl and propargyl) reacted together to form 3-butynylbenzene and 2,3-butadienylbenzene. The addition reaction was barrierless, and the reaction energies for the two possible adducts were 279 and 282 kJ/mol, which are comparable to the reaction energy for IS1 formation. A hydrogen abstraction from the aromatic ring of IS1 by H atom requires an activation energy of 70.1 kJ/mol to form IS2. The free radical site on one of the aromatic ring in IS2 may attack the other ring to form a fused 3-ring structure, IS3. This ring formation requires an activation energy

barrier of 14.0 kJ/mol to be overcome. The H-elimination from the 4a-carbon site of IS3 forms IS4 (9,10-dihydrophenanthrene). Four possible routes for IS4 are shown in the figure, and are described below as *Routes a-d*.

Route a: This route, shown by solid lines, requires H-abstraction from one of the CH₂-sites of IS4 to form IS5. Thereafter, with the release of another H-atom from adjacent CH₂-site, phenanthrene is formed, which lies 242.4 kJ/mol below the energy of two benzyl radicals (i.e. the reactants).

Route b: Shown by dotted lines, this route involves the elimination of H₂ from one of the CH₂-sites of IS4 to form IS6. This requires a high activation energy of 404.1 kJ/mol. The intermediate species, IS6, then undergoes H-migration from the CH₂-site to the free radical site to form phenanthrene.

Route c: Shown by dashed lines, this route also requires H₂ elimination to form phenanthrene from IS4 through the removal of one H-atom each from the two CH₂-sites, and involves overcoming an energy barrier of 436.7 kJ/mol.

Route d: Shown by dash-dotted line, this route involves H-desorption from IS4 to form IS5. This is a unimolecular reaction, and unlike *Route a*, does not require any external H atom. However, a high energy barrier of 433.9 kJ/mol is required to be overcome to break the C-H bond in IS4.

Similar to IS4 → IS6 + H₂ and IS4 → phenanthrene + H₂, several reactions in this paper involve H₂ elimination through the loss of two H atoms from the same C atom or from two adjacent C atoms. Such H₂ elimination reactions have been studied by Irle *et*

*al.*⁴⁷ for aliphatic hydrocarbons, methane, ethane and propane. It was found that, for the removal of two H atoms from same C atom to form H₂, energy barriers of 485.8 kJ/mol for methane, 441.8 kJ/mol for ethane, and 436.4 kJ/mol for terminal C-atoms and 407.1 kJ/mol for central C-atom of propane were required, which are comparable to 404.1 kJ/mol required for IS4 → IS6 + H₂. For the simultaneous loss of two H atoms from two adjacent C atoms, energy barriers of 476.9 kJ/mol for ethane, and 475.7 kJ/mol for propane were required, which are also comparable to 436.7 kJ/mol observed for IS4 → phenanthrene + H₂.

3.2. Pathway 2

Similar to Pathway 1, this pathway also involves H-loss from IS1, but from the aliphatic chain to form IS7. Figure 4 presents the potential energy diagram for this pathway. The species, IS7 can be formed through H-abstraction from IS1 by another H atom, or through the direct desorption of H atom from IS1. The H-abstraction from the aliphatic chain requires a small activation energy of 28.7 kJ/mol, which is lower than the activation energy required for IS1 + H → IS2 + H₂. The low energy requirement for H-abstraction from aliphatic chain as compared to aromatic ring is well explained in⁴⁸. For H-desorption, a high energy barrier of 450 kJ/mol is involved. The possible reactions of IS7 are explained below as *routes a-e*.

Route a: In IS7, H-migration from the aromatic ring to the free radical site can take place to form IS2 after overcoming an energy barrier of 274.6 kJ/mol. The further reaction of IS2 is already explained in Pathway 1.

Route b: The desorption of H-atom from the aliphatic chain of IS7 forms *e*-stilbene (IS8) after overcoming an energy barrier of 168.8

kJ/mol. The species, IS8, can then follow two sub-routes: (i) IS8 → IS9 (represented by thick solid lines), and (ii) IS8 → IS11 (represented by thin solid lines).

In sub-route (i), IS9 is formed through H-abstraction from one of the aromatic rings in IS8 by H atom. The free radical site, thus formed, attacks a C atom on the other ring to form a fused 3-ring structure, IS10, lying 139.5 kJ/mol below IS9. The removal of H atom from the 4b-carbon of IS10 requires an activation energy of 80.0 kJ/mol, and leads to the formation of phenanthrene. From IS9, a structure with 4-membered ring, IS14, can also form, but it requires a high energy barrier of 114.2 kJ/mol. A C-C bond in the 4-membered ring of IS14 breaks to form IS15. The dangling C-H radical then attacks a nearby carbon to form IS16, which lies 197.4 kJ/mol below IS15. The removal of H atom from IS16 forms anthracene (IS17).

In sub-route (ii), the H-abstraction from the aliphatic chain of IS8 forms IS11, and requires an activation energy of 66.5 kJ/mol. A ring closure reaction then takes place to form a fused ring structure, IS12, which lies 160.7 kJ/mol above IS11. The next step involves bond rearrangement to form IS13. From this species, the H-migration from 4a-carbon to 10-carbon forms IS10 (detailed above), and the loss of H₂-molecule (through the loss of H atoms from carbons at 4a and 4b-positions) forms IS18. The addition of H atom to IS18 then forms phenanthrene.

Route c: In this route, represented by solid lines in Figure 5, IS7 undergoes ring closure reaction to form a 3-ring structure, IS19, after overcoming a potential energy barrier of 172.8 kJ/mol. There are two possibilities for the species, IS19. It can form IS20 through the loss of H-atom from 4a-site. This is followed by H-elimination reactions from 4b-carbon site in IS20, and 10-carbon site in IS21, to

ARTICLE

Physical Chemistry Chemical Physics

eventually form phenanthrene. The removal of H-atom from 10-carbon site in IS20 leads to IS10 formation after overcoming an energy barrier of 309.5 kJ/mol, which forms phenanthrene through the loss of H atom.

The species IS19, formed in this route, can also undergo H-desorption from 10-carbon site to form an intermediate species, 4a,4b-dihydrophenanthrene (IS22), lying 211.6 kJ/mol above IS19. The activation energy required for IS19 \rightarrow IS22 is higher than that for IS19 \rightarrow IS20 by 108.1 kJ/mol, thus making the latter one preferable over the former one. From IS22, the elimination of two H atoms from 4a and 4b-carbons to form phenanthrene requires an activation energy of 257.7 kJ/mol.

Route d: Shown by dashed lines in Figure 5, this route involves the conversion of IS7 to IS23 with fused 4-membered and 6-membered rings after overcoming an energy barrier of 148.6 kJ/mol. This is followed by the formation of a 5-membered ring in IS24, which lies 232.3 kJ/mol above IS23. Thereafter, IS24 undergoes H-elimination reaction to form IS25. The loss of another H atom from IS25 forms the intermediate species, IS26 which lies 218.6 kJ/mol above it. The fused 4-membered ring in IS26 then breaks to form IS27 after overcoming an energy barrier of 118.5 kJ/mol. The species, IS27 undergoes H-migration reaction to form IS28. The dangling CH₂ group forms a 3-membered ring structure in IS29 after overcoming an energy barrier of 230.1 kJ/mol. The migration of H atom takes place from the CH₂-site of IS29 to the nearby C-atom to form IS30. The bond connecting the fused 5-membered and 3-membered ring in IS30 breaks to form IS10, which requires overcoming a small potential energy barrier of 10.6 kJ/mol. Phenanthrene is then formed from it, as explained before.

Route e: Figure 6 presents the potential energy diagram of this route for IS7 decomposition involving IS31 formation with fused 3-membered and 6-membered rings. For IS7 \rightarrow IS31, an energy barrier of 214.2 kJ/mol is required to be overcome. Thereafter, H-desorption from IS31 leads to the formation of IS32, lying 168.2 kJ/mol above it. The abstraction of H atom from IS32 gives rise to another radical species, IS33. A ring closure reaction in IS33 forms IS34, lying 90.7 kJ/mol below IS33. A C-C bond in the tricyclic ring of IS34 breaks to form IS35. This is followed by H-migration from 8-carbon site to 8a-carbon site in IS35 to form IS36. Another H-migration reaction from 9-carbon site to 10-carbon site in IS36 after overcoming an energy barrier of 129.2 kJ/mol forms IS10, which leads to phenanthrene formation through the loss of H atom.

In this figure, the energies of anthracene and phenanthrene can be compared. Phenanthrene has lower energy than anthracene by 23 kJ/mol as per CBS-QB3 calculations (and 21.4 kJ/mol from B3LYP/6-311++G(d,p) calculations). This observation is in line with the detailed study on straight and kinked polycyclic benzenoids by Poater et al.⁴⁹, where the stabilizing interaction in π -electron system leading to better π bonding in phenanthrene was found to be responsible for its higher stability despite H-H repulsion at its armchair site.

3.3. Pathway 3

The potential energy diagram of Pathway 3 is presented in Figure 4. This pathway involves the removal of H₂ molecule from the α - and β -carbon of IS1 after overcoming an energy barrier of 448.5 kJ/mol to form IS8 lying 90.2 kJ/mol above it. The further reactions of IS8 are already described in Pathway 2.

3.4. Pathway 4

Figure 7 presents the potential energy diagram for Pathway 4 involving IS37 formation from IS1 through H₂-elimination from one of its aliphatic carbon. This H₂ elimination reaction involves an activation energy of 415.2 kJ/mol. For the further reactions of IS37, four routes are proposed, as described below as *Routes a-d*.

Route a: This route, represented by thick solid lines, involves the migration of H atom from one of the aliphatic carbon site of IS37 to another to form IS8. This migration reaction requires an activation energy of 128.6 kJ/mol to be overcome. The further reactions of IS8 have already been discussed in Pathway 2.

Route b: This route, represented by thin solid lines, involves H-migration from one of the aromatic carbon in IS37 to the free radical site on aliphatic chain to form IS38 after overcoming an energy barrier of 182.6 kJ/mol. A ring closure reaction follows, which results in the formation of fused 3-membered and 6-membered rings in IS32. The further reactions for IS32 are discussed before.

Route c: Shown by dotted lines, this route involves a ring closure reaction in IS37 to form a 4-membered ring in IS39 after overcoming an energy barrier of 87.5 kJ/mol. This is followed by the formation of a 5-membered ring in IS40, which involves an activation energy of 283.8 kJ/mol. As evident from the energy diagram, high energies are involved in this route, which makes it unfavourable. One of the C-C bond in the 4-membered ring of IS40 breaks to form a dangling CH₂-group on the 5-membered ring in IS41. The migration of H atom between the free radical site on the 6-membered ring and the fused 5-membered ring in IS41 takes

place to form IS42 that lies 194.1 kJ/mol below IS41. The dangling CH₂-group then forms a 3-membered ring fused with the 5-membered ring in IS43. Thereafter, the C-C bond connecting the 3-membered and the 5-membered rings breaks to form a 6-membered ring between the two benzene rings in species, IS44, which is more stable than IS43. The H-migration from the 9-carbon site to the 10-carbon site forms IS22, which then forms phenanthrene through H₂ elimination.

Route d: Represented by dashed lines, in this route, IS37 undergoes a ring closure reaction to form IS44. An energy barrier of 159.3 kJ/mol is required to be overcome for this reaction. The further reactions of IS44 are already discussed before.

3.5. Reaction Rate constants

Table S1 in the supplementary material provides the high-pressure limit rate constants of the elementary reactions involved in the formation of phenanthrene and anthracene from benzyl recombination. For the barrierless addition reaction, 2benzyl ↔ IS1, the variational transition state theory was used to calculate the rate constant by determining the potential energy surface through partial geometry optimizations at different C-C bond lengths. The method is described in our previous works^{50, 51}. Figure 8 provides the rate constant for some important reactions. In Figure 8(a), the experimentally observed⁵²⁻⁵⁴, computed, and literature-based³⁶ rate constants for benzyl recombination to form IS1 are provided. In experimental studies, the rate constant for benzyl recombination was found to have very weak pressure dependence. The computed rate constants were obtained in this work at two levels of theory: CBS-QB3 and B3LYP/6-311++G(d,p). It can be seen in Figures 8(a) that the rate constant from CBS-QB3 (represented by solid line in

ARTICLE

Physical Chemistry Chemical Physics

black colour) matches very well with different sets of experimental data represented by bullet points. Note that the literature-based rate constant for this reaction in ³⁶ was obtained by fitting Arrhenius equation to an experimental data. This is why, it overlaps with one set of experimental data. Figure 8(b) provides the computed rate constants using CBS-QB3 for various reactions through which IS1 can decompose to form IS2, IS7, IS8, IS37 and benzyl radicals. The experimentally observed rate constant for the reverse reaction, $IS1 \rightarrow 2benzyl$, obtained from ⁵⁴, are also provided. A good match between the computed and the experimentally observed rates (represented by black solid line and bullet points, respectively) for this reaction was found. The rate constant used in Qi et al. ³⁶ for this reaction is also provided in this figure. It can be seen that the rate constant for this reaction was under-estimated in their work. Out of six reactions listed in this figure for IS1 decomposition, the ones involving H-abstraction by H atoms had higher rate constants than the unimolecular reactions. Out of the four unimolecular reactions, $IS1 \rightarrow 2benzyl$ had highest rate constant. This indicates that, in a combustion environment, where the rates of the reactions for H-abstraction from IS1 are not very high, IS1 may decompose back to the reactants (benzyl radicals). The experimental data in the literature were available for very few aromatic reactions relevant to this study and over narrow temperature ranges. This restricted the number of validation cases for reaction kinetics.

3.6. Mechanism analysis

To determine the major products formed through benzyl recombination and the preferred pathways for their formation, simulations were carried out using Logesoft software ⁵⁵ by including all the elementary reaction proposed in this work. The reactions

were studied in a closed homogeneous zero-dimensional reactor with a simplified reactor feed containing 0.1, 0.1, 10, and 89.8 mol% of benzyl, H, H₂, and N₂, respectively. These concentrations of benzyl, H and H₂ reflect very well their typical concentrations in hydrocarbon flames ^{56, 57}. The simulations were performed at different temperatures for a residence time of 0.1s and at a pressure of 1 atm. The rate-of-production analysis was used to determine the reactions responsible for the formation of a given product ¹⁰.

Figure 9 provides the mole fractions of benzyl, H, phenanthrene, IS1, IS7 and anthracene that were present in considerable amounts in the reactor at temperatures of 1000, 1500, and 2000 K. In Figure 9(a), the final benzyl concentrations increased with increasing temperature, indicating that benzyl recombination becomes less favourable as the temperature is increased. However, even at the temperature of 2000 K, the final mol fraction of benzyl remained much lower than the initial mole fraction of 10^{-3} . The mole fraction of H atom was found to decrease with increasing time at 1000 K, but at 1500 and 2000 K, it remained almost constant at all times. This will be explained later. Figure 9(b) presents the mole fraction profiles of two main products, phenanthrene and anthracene. As evident, anthracene concentration remained negligible (with mole fraction of 1.7×10^{-6}) even at a high temperature of 2000 K. Phenanthrene mole fraction was significantly low at 1000 K. However, at 1500 and 2000 K, its final mole fraction reached near its maximum value of 5×10^{-4} . Figure 9(c) presents the mole fraction profiles of IS1 and IS7. The species IS1 was a short lived intermediate with low concentrations at all the temperatures. Though the species, IS7 (a resonantly stabilized radical) with the final mole fraction of about 5×10^{-4} was the main product at 1000 K, its final concentration decreased drastically at

higher temperatures of 1500 and 2000 K. The decrease in the concentration of H atom, as observed in Figure 9(a) at 1000 K, was a result of its involvement in forming IS7 (through $IS1 + H \rightarrow IS7 + H_2$) that was not decomposing into any other species at that temperature. However, at higher temperatures (1500 and 2000 K), when phenanthrene was the main product, H concentrations remained almost constant because its rate of consumption (through $IS1 + H \rightarrow IS7 + H_2$ and $IS4 + H \rightarrow IS5 + H_2$) became similar to its rate of production through ($IS3 \rightarrow IS4 + H$ and $IS5 \rightarrow \text{phenanthrene} + H$). The decrease in IS7 mole fraction at 1500 and 2000 K correlates with increase in phenanthrene concentration at those temperatures due to its significant role in phenanthrene formation. The simulations at temperatures in between 1000-1500 K revealed that IS7 is converted to phenanthrene at temperatures above 1200 K (not shown in the figure).

Through the rate-of-production analysis, the main reactions leading to phenanthrene formation were found, and are shown in Figure 10. This channel for phenanthrene formation was found to remain unchanged at all the temperatures in between 500 and 2000 K. The other reactions in the detailed mechanism were found to have negligible effect on its concentration. Though the concentration of anthracene remained very low at all the temperatures considered in this work, its formation took place due to phenanthrene decomposition through these reactions: $\text{phenanthrene} + H \rightarrow IS10 \rightarrow IS9 \rightarrow IS14 \rightarrow IS15 \rightarrow IS16 \rightarrow \text{anthracene} + H$.

To assess the effect of DFT functionals on the reaction energetics, the reactions present in the reduced mechanism in Figure 10 were studied using M062X functional. It can be seen in Table S3 of the supplementary material that the energies obtained from this functional is closer to the energies from CBS-QBS as

compared to those from the B3LYP functional. This further confirms the finding in Section 3.5 that B3LYP may not be the best choice for aromatic reactions, and a systematic study on the comparison of different DFT functionals for large aromatics, similar to the one presented in⁵⁸, is required.

3.7. Flame simulations

To determine the effect of the proposed reactions in Figure 10 for phenanthrene formation from benzyl radicals on the profiles of phenanthrene and other species in flames, two premixed laminar toluene flames, experimentally observed in^{57, 59}, were simulated. For simulations, a toluene mechanism, developed in³⁶, was used as the base mechanism. This base mechanism already had reactions for phenanthrene formation from benzyl. Therefore, for each flame, three simulations were performed using: (a) the base mechanism, (b) the mechanism where the reactions in the base mechanism for phenanthrene formation from benzyl were replaced with the reactions suggested in this work, and (c) the mechanism where no reactions for phenanthrene formation from benzyl recombination were considered. Figure 11 presents the experimental and three simulated profiles of species in two toluene flames. The experimental conditions of the two flames are provided in the figure caption. The modifications in the mechanism mainly affected phenanthrene concentration in both the flames. With the base mechanism, phenanthrene mole fraction was over-predicted due to underestimated rate constant for bibenzyl decomposition to form benzyl radicals, and over-estimated rate constants for the dehydrogenation of the intermediate species (that eventually were forming phenanthrene). With the reactions suggested in this work, the match between the experimental and the simulated profiles improved, but a slight under-prediction is observed. Without benzyl

ARTICLE

Physical Chemistry Chemical Physics

recombination reactions, phenanthrene mole fraction is noticeably under-predicted.

In general, the experimental profiles of the aromatic species (benzene, naphthalene and phenanthrene) appeared to be shifted towards left as compared to the simulated profiles for both the flames. This could be due to the disturbance of the flames upon the insertion of the sampling probe that led to some inaccuracies in the minor species profiles. To further improve the match between the experimental and the simulated results for aromatics, detailed studies similar to this work on the other important aromatic reactions present in the mechanism should be conducted in the future to improve their kinetics.

Conclusions

A reaction mechanism for the self-addition of benzyl to form three-ring aromatic hydrocarbons, phenanthrene and anthracene, was developed. The molecular geometries and energetics were obtained using B3LYP/6-311++G(d,p) and CBS-QB3 levels of theory. Benzyl self-addition reaction, leading to bibenzyl formation, was found to be barrierless and exothermic with a reaction energy 283.2 kJ/mol from CBS-QB3 calculations. The calculated rate constant for this reaction agreed very well with different sets of experiment data from the literature. The further reactions of bibenzyl involved H-abstraction by H atom from the aliphatic chain or from the aromatic rings, and H or H₂-desorption from the aliphatic chain without the use of any external H atom. From the rate constants for the possible decomposition reactions for bibenzyl, it was found that the routes involving H-abstraction by H atom to create a radical site on bibenzyl and the reverse reaction to form the reactants (benzyl radicals) were competitive, while the reaction involving the desorption of H or H₂ had very low rate constants at all the

temperatures in between 300-3000 K. Through mechanism analysis at different temperatures, it was concluded that phenanthrene is the main product of benzyl self-addition at temperatures above 1200 K. As the temperature increased, the increase in the rate of reverse reaction involving bibenzyl decomposition to benzyls decreased the rate of increase in phenanthrene concentration. A reduced mechanism with seven important reactions for phenanthrene formation was proposed. These reactions, when included in toluene oxidation mechanism, improved the model prediction of phenanthrene concentrations in two premixed laminar flames.

Supplementary Material

The rate constants of the elementary reactions, and the energies, coordinates, vibrational frequencies, moments of inertia, and spin multiplicity for all the intermediate species and transition states are provided in the supplementary material.

Acknowledgments

This work has been financially supported by the Petroleum Institute, Abu Dhabi, UAE.

References

1. M. Z. Jacobson, *Nature*, 2001, **409**, 695.
2. A. Raj, Formation, growth and oxidation of soot: a numerical study, University of Cambridge, 2010.
3. A. Raj, M. Sander, V. Janardhanan and M. Kraft, *Combust. Flame*, 2010, **157**, 523.

4. K. H. Homann and H. G. Wagner, Some new aspects of the mechanism of carbon formation in premixed flames, in *Symposium (International) on Combustion*, 1967, pp. 371.
5. B. Crittenden and R. Long, *Combust. Flame*, 1973, **20**, 359.
6. H. Bockhorn, F. Fetting and H. Wenz, *Ber. Bunsen-Ges. Phys. Chem.*, 1983, **87**, 1067.
7. M. Frenklach, D. W. Clary, W. C. Gardiner and S. E. Stein, Detailed kinetic modelling of soot formation in shock-tube pyrolysis of acetylene, in *Symposium (International) on Combustion*, 1985, pp. 887.
8. P. R. Westmoreland, A. M. Dean, J. B. Howard and J. P. Longwell, *J. Phys. Chem.*, 1989, **93**, 8171.
9. N. Marinov, W. Pitz, C. Westbrook, M. Castaldi and S. Senkan, *Combust. Sci. Technol.*, 1996, **116**, 211.
10. A. Raj, I. D. C. Prada, A. A. Amer and S. H. Chung, *Combust. Flame*, 2012, **159**, 500.
11. Y. Wang, A. Raj and S. H. Chung, *Combust. Flame*, 2013, **160**, 1667.
12. A. Raj, M. J. Al Rashidi, S. H. Chung and S. M. Sarathy, *J. Phys. Chem. A*, 2014, **118**, 2865.
13. A. Violi, A. D'Anna and A. D'Alessio, *Chem. Eng. Sci.*, 1999, **54**, 3433.
14. B. Shukla, A. Miyoshi and M. Koshi, *J. Am. Soc. Mass. Spectrom.*, 2010, **21**, 534.
15. B. Shukla and M. Koshi, *Phys. Chem. Chem. Phys.*, 2010, **12**, 2427.
16. J. A. Miller and C. F. Melius, *Combust. Flame*, 1992, **91**, 21.
17. C. McEnally and L. Pfefferle, *Combust. Sci. Technol.*, 1998, **131**, 323.
18. U. Alkemade and K. Homann, *Z. Phys. Chem. (Muenchen, Ger.)*, 1989, **161**, 19.
19. R. S. Tranter, X. Yang and J. H. Kiefer, *P. Combust. Inst.*, 2011, **33**, 259.
20. J. A. Miller and S. J. Klippenstein, *J. Phys. Chem. A*, 2003, **107**, 7783.
21. Y. Georgievskii, J. A. Miller and S. J. Klippenstein, *Phys. Chem. Chem. Phys.*, 2007, **9**, 4259.
22. A. D'Anna, A. D'Alessio and J. Kent, *Combust. Flame*, 2001, **125**, 1196.
23. M. Lu and J. A. Mulholland, *Chemosphere*, 2001, **42**, 625.
24. A. D'anna and A. D'Alessio, *Combust. Flame*, 2000, **121**, 418.
25. A. Gomez, G. Sidebotham and I. Glassman, *Combust. Flame*, 1984, **58**, 45.
26. D. H. Kim, J.-K. Kim, S.-H. Jang, J. A. Mulholland and J.-Y. Ryu, *Environ. Eng. Res.*, 2007, **12**, 211.
27. A. Matsugi and A. Miyoshi, *Int. J. Chem. Kinet.*, 2012, **44**, 206.
28. R. Spielmann and C. Cramers, *Chromatographia*, 1972, **5**, 295.
29. A. Violi, A. D'Anna, A. D'Alessio and A. F. Sarofim, *Chemosphere*, 2003, **51**, 1047.
30. A. Violi, A. Sarofim and T. Truong, *Combust. Flame*, 2001, **126**, 1506.
31. A. Lamprecht, B. Atakan and K. Kohse-Höinghaus, *P. Combust. Inst.*, 2000, **28**, 1817.
32. M. Colket and D. Seery, Reaction mechanisms for toluene pyrolysis, in *Symposium (International) on Combustion*, 1994, pp. 883.
33. N. Marinov, W. Pitz, C. Westbrook, A. Lutz, A. Vincitore and S. Senkan, Chemical kinetic modelling of a methane opposed-flow diffusion flame and comparison to experiments, in *Symposium (International) on Combustion*, 1998, pp. 605.
34. S. Sinha, A. Raj, A. S. AlShoabi, S. M. Alhassan and S. H. Chung, *Ind. Eng. Chem. Res.*, 2014, **53**, 16293.

ARTICLE

Physical Chemistry Chemical Physics

35. M. J. Castaldi, N. M. Marinov, C. F. Melius, J. Huang, S. M. Senkan, W. J. Pitt and C. K. Westbrook, Experimental and modeling investigation of aromatic and polycyclic aromatic hydrocarbon formation in a premixed ethylene flame, in *Symposium (International) on Combustion*, 1996, pp. 693.
36. L. Zhang, J. Cai, T. Zhang and F. Qi, *Combust. Flame*, 2010, **157**, 1686.
37. H. Hippler and J. Troe, *J. Phys. Chem.*, 1990, **94**, 3803.
38. M. Sander, A. Raj, O. Inderwildi, M. Kraft, S. Kureti and H. Bockhorn, *Carbon*, 2009, **47**, 866.
39. A. Raj, P. L. Man, T. S. Totton, M. Sander, R. A. Shirley and M. Kraft, *Carbon*, 2010, **48**, 319.
40. A. Raj, Z. Zainuddin, M. Sander and M. Kraft, *Carbon*, 2011, **49**, 1516.
41. K. Wang, S. M. Villano and A. M. Dean, *Phys. Chem. Chem. Phys.*, 2015, **17**, 6255.
42. T. Seta, M. Nakajima and A. Miyoshi, *J. Phys. Chem. A*, 2006, **110**, 5081.
43. J. M. Simmie and K. P. Somers, *J. Phys. Chem. A*, 2015, **119**, 7235.
44. M. Frisch, G. Trucks, H. Schlegel, G. Scuseria, M. Robb, J. Cheeseman, G. Scalmani, V. Barone, B. Mennucci and G. Petersson, Gaussian 09; Gaussian, Inc.: Wallingford, CT, 2009.
45. A. Gonzalez-Lafont, T. N. Truong and D. G. Truhlar, *J. Phys. Chem.*, 1991, **95**, 4618.
46. R. L. Bell and T. N. Truong, *J. Chem. Phys.*, 1994, **101**, 10442.
47. S. Irle and K. Morokuma, *J. Chem. Phys.*, 2000, **113**, 6139.
48. S. J. Blanksby and G. B. Ellison, *Acc. Chem. Res.*, 2003, **36**, 255.
49. J. Poater, R. Visser, M. Sola and F. M. Bickelhaupt, *J. Org. Chem.*, 2007, **72**, 1134.
50. S. Sinha, A. Raj, A. S. AlShoaibi, S. M. Alhassan and S. H. Chung, *Ind. Eng. Chem. Res.*, 2014, **53**, 10608.
51. A. Raj, G. R. da Silva and S. H. Chung, *Combust. Flame*, 2012, **159**, 3423.
52. K. Luther, K. Oum, K. Sekiguchi and J. Troe, *Phys. Chem. Chem. Phys.*, 2004, **6**, 4133.
53. A. Boyd, B. Noziere and R. Lesclaux, *J. Phys. Chem.*, 1995, **99**, 10815.
54. W. Müller-Markgraf and J. Troe, *J. Phys. Chem.*, 1988, **92**, 4899.
55. LOGEsoft v. 1.02. In: Engineering, L.C. (ed.) (2014).
56. R. I. Singh, A. M. Mebel and M. Frenklach, *J. Phys. Chem. A*, 2015.
57. W. Yuan, Y. Li, P. Dagaut, J. Yang and F. Qi, *Combust. Flame*, 2015, **162**, 22.
58. D. R. Brittain, C. Y. Lin, A. T. Gilbert, E. I. Izgorodina, P. M. Gill and M. L. Coote, *Phys. Chem. Chem. Phys.*, 2009, **11**, 1138.
59. Y. Li, J. Cai, L. Zhang, T. Yuan, K. Zhang and F. Qi, *P. Combust. Inst.*, 2011, **33**, 593.

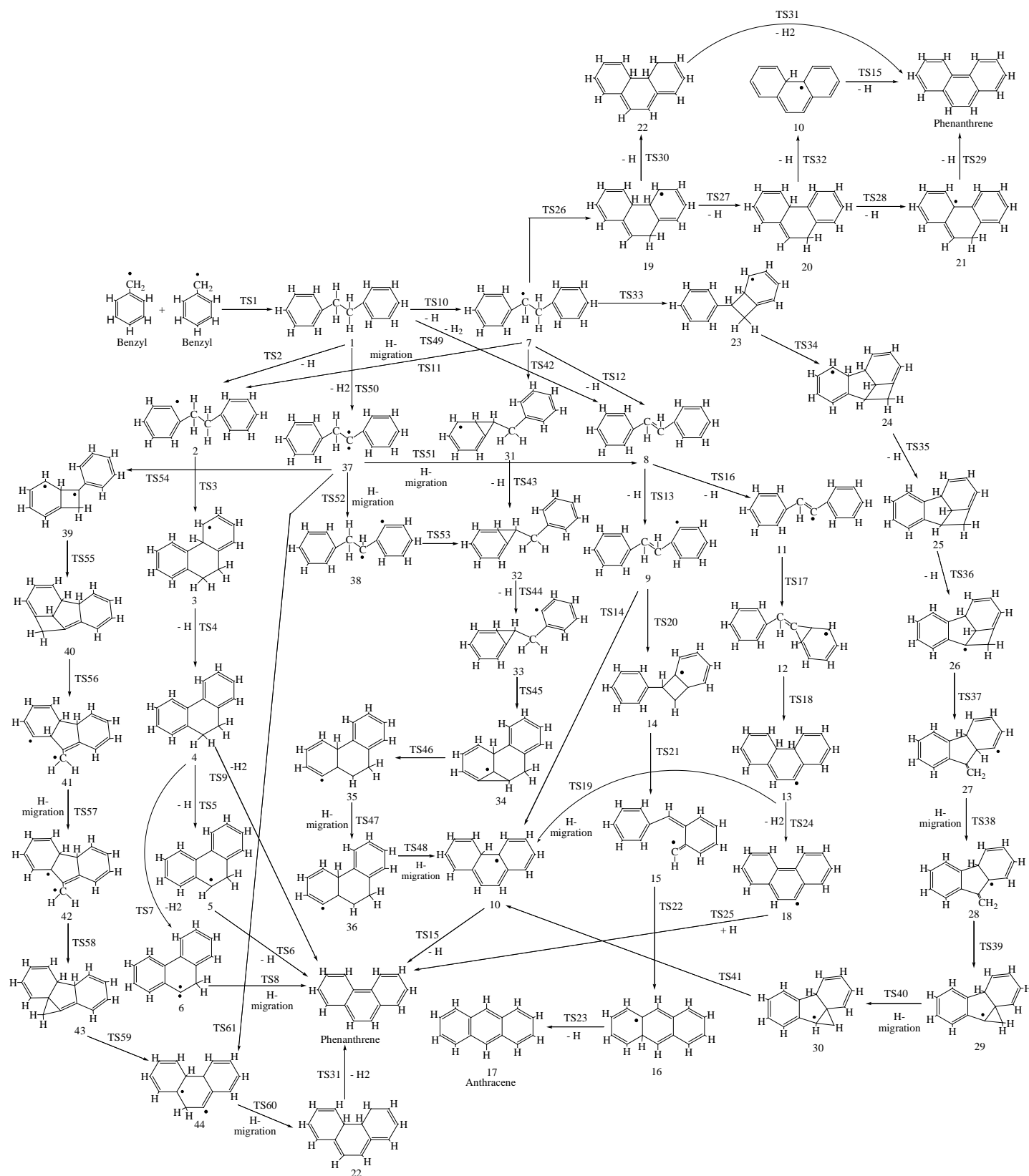


Figure 1: Reaction mechanism for the formation of phenanthrene and anthracene through self-addition of benzyl radicals.

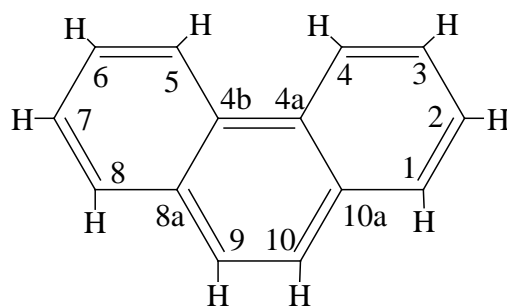


Figure 2: Phenanthrene with numbered C atoms to assist in the discussion of reaction mechanism.

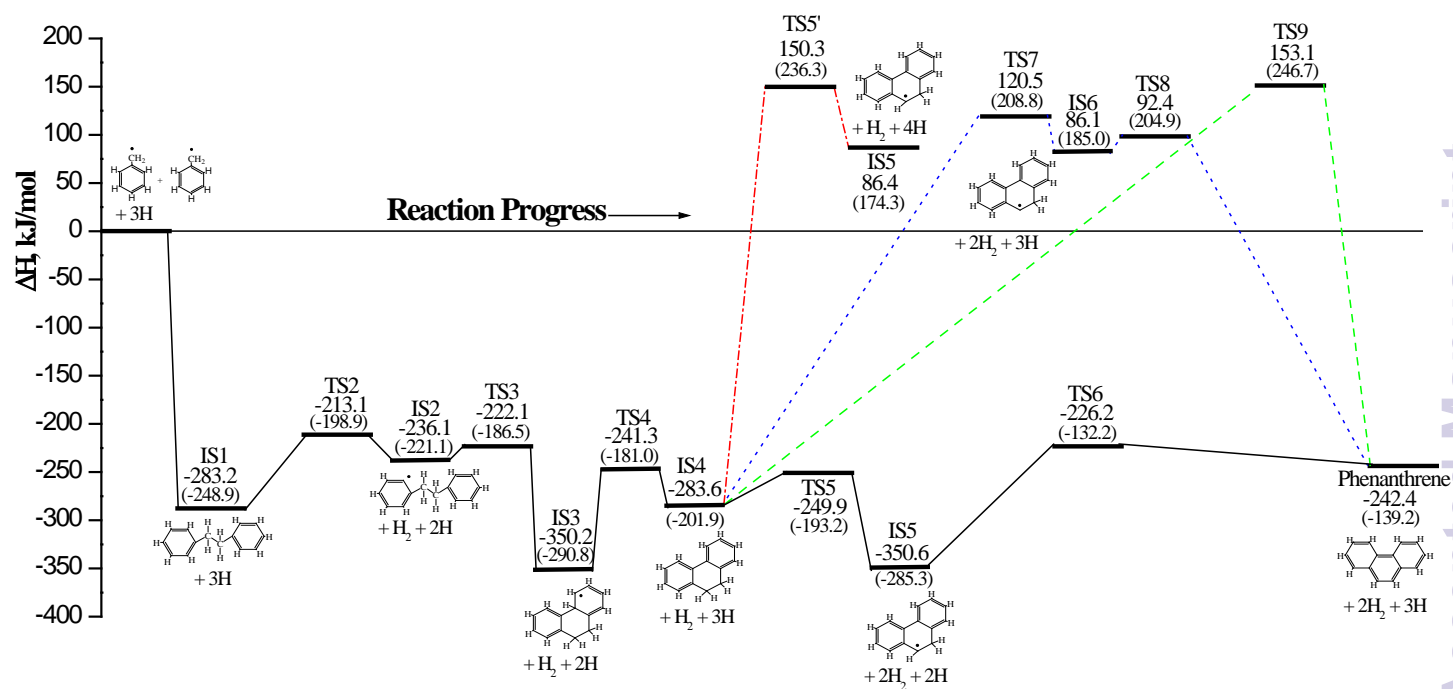


Figure 3: Potential energy diagram for Pathways 1 involving bibenzyl decomposition through H-abstraction reaction to the form phenanthrene with the energies obtained from CBS-QB3 calculations. The energies in the bracket were obtained using B3LYP/6-311++G(d,p).

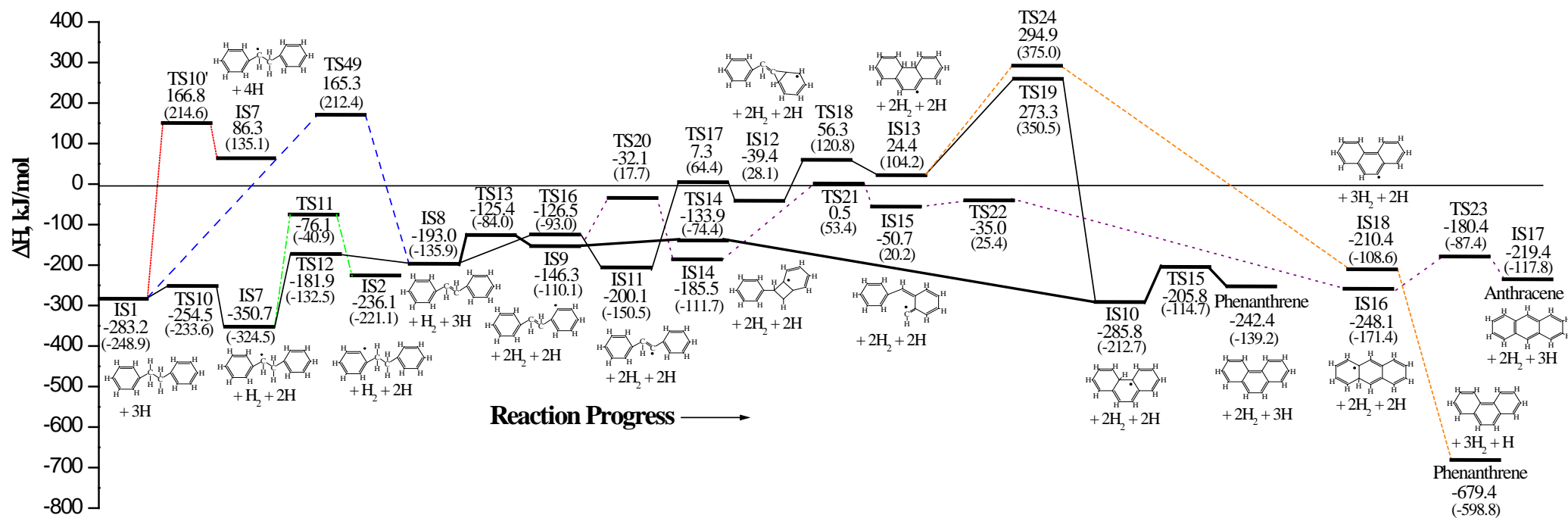


Figure 4: Potential energy diagram for Pathway 2 involving IS7 formation from IS2 and its decomposition to form phenanthrene with the energies obtained from CBS-QB3 calculations. The energies in the bracket were obtained using B3LYP/6-311++G(d,p).

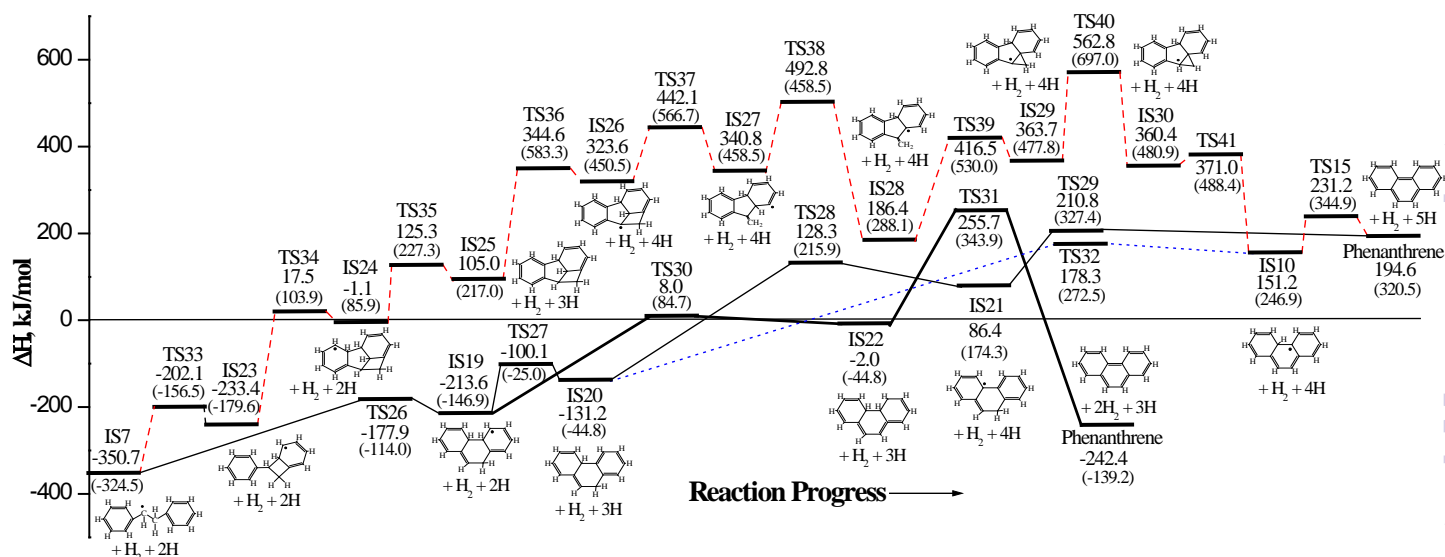


Figure 5: Potential energy diagram of two routes (IS7 → IS19) and (IS7 → IS23) for the decomposition of IS7 to form phenanthrene with the energies obtained from CBS-QB3 calculations. The energies in the bracket were obtained using B3LYP/6-311++G(d,p).

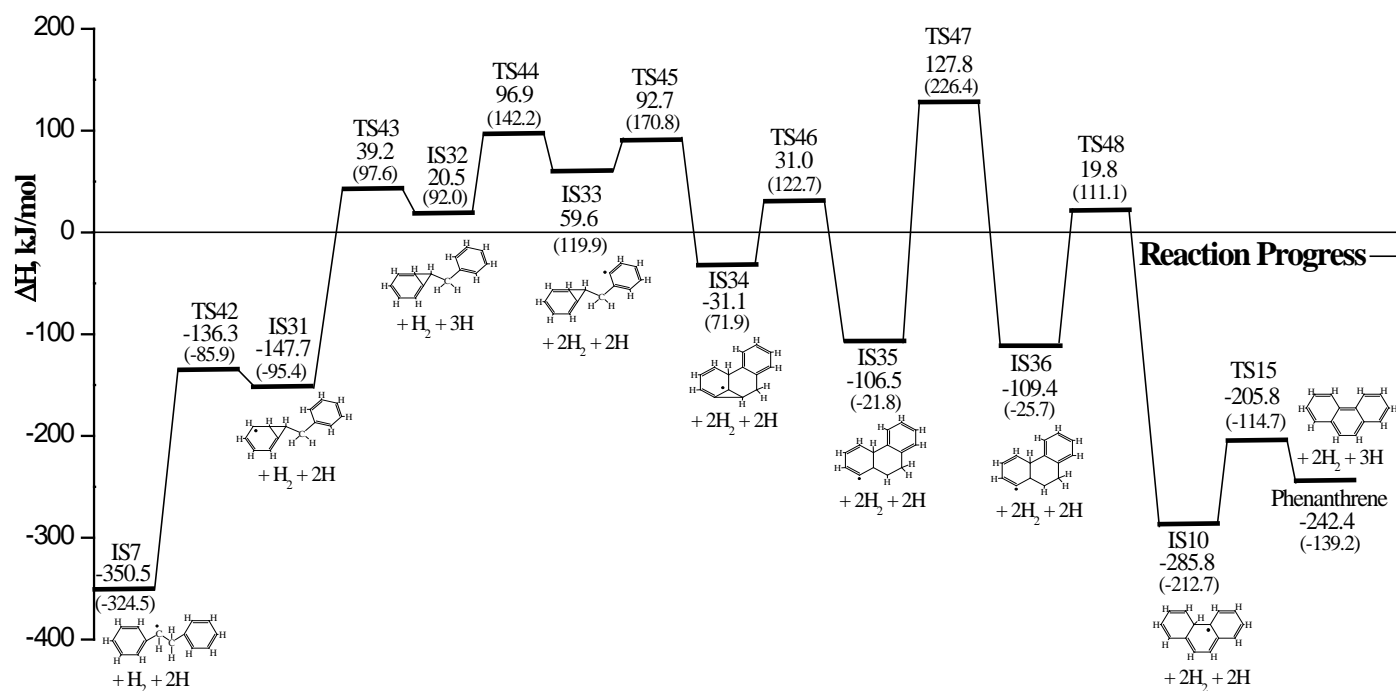


Figure 6: Potential energy diagram of a route for IS7 decomposition leading to phenanthrene formation with the energies obtained from CBS-QB3 calculations. The energies in the bracket were obtained using B3LYP/6-311++G(d,p).

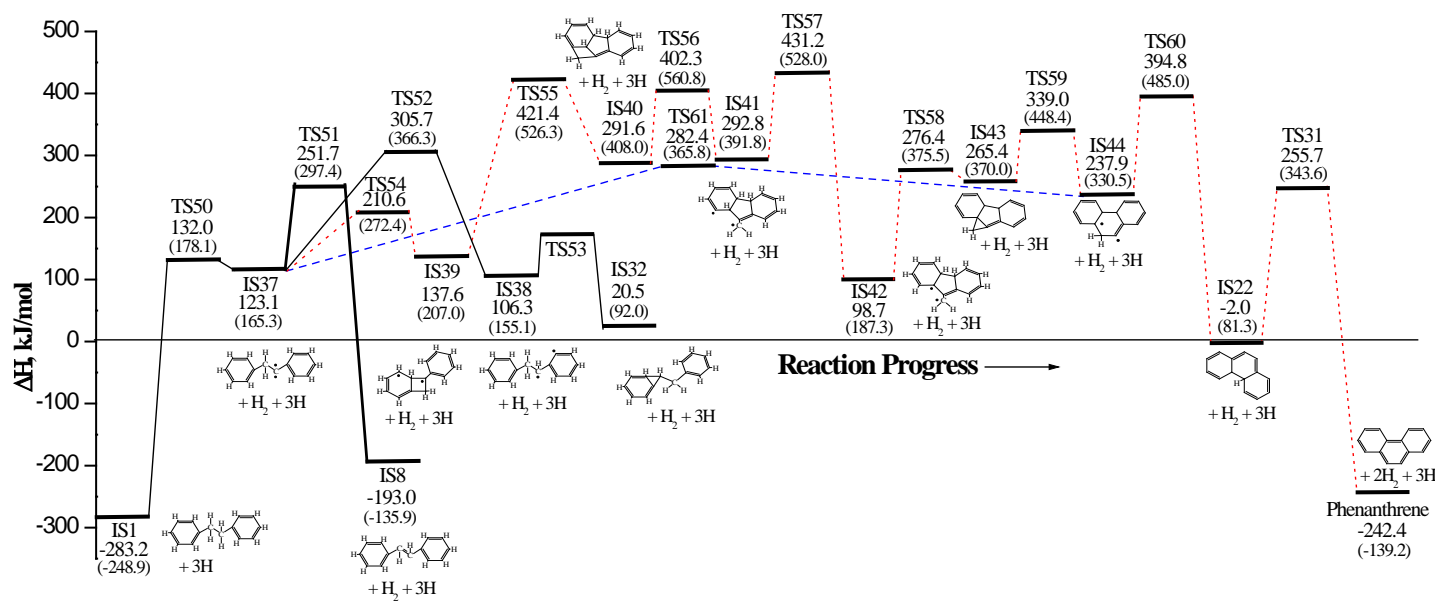


Figure 7: Potential energy diagram for Pathway 4 for phenanthrene formation from IS1 with the energies obtained from CBS-QB3 calculations. The energies in the bracket were obtained using B3LYP/6-311++G(d,p).

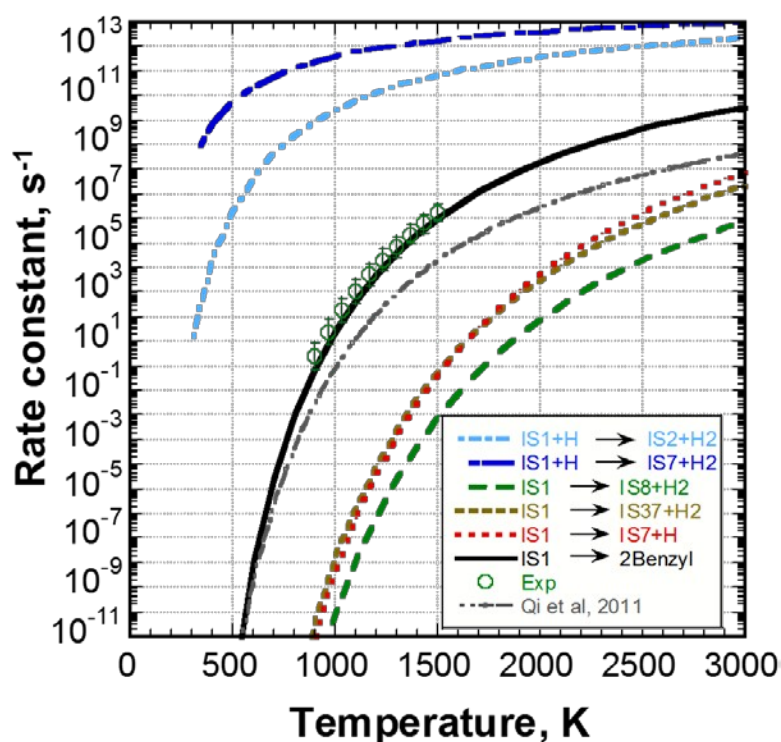
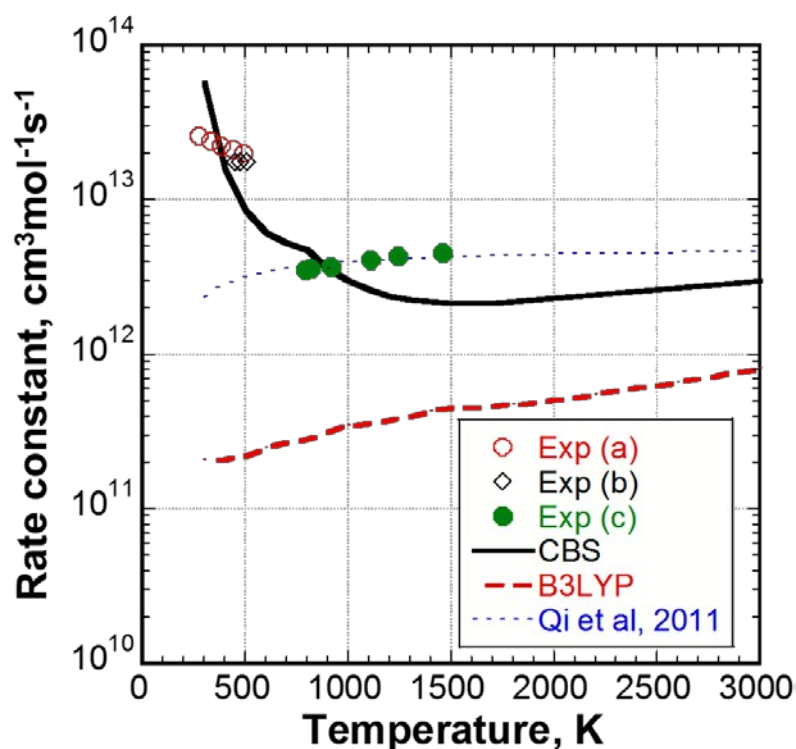
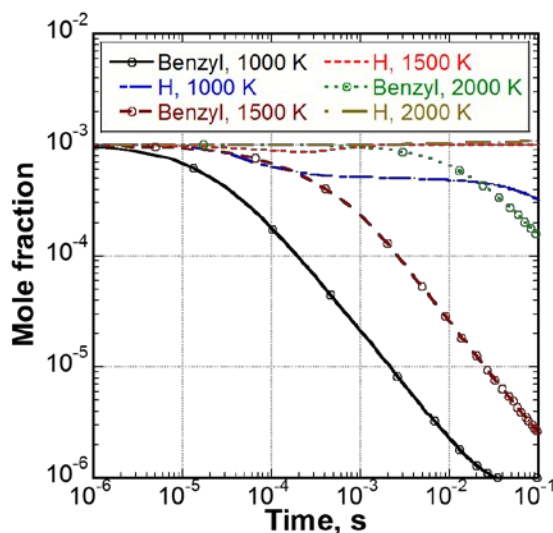
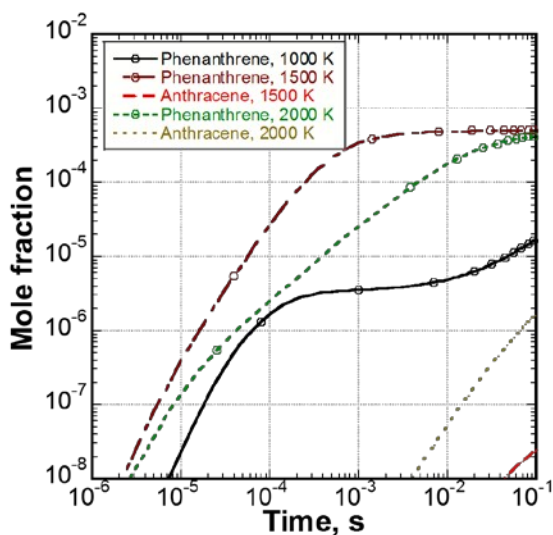


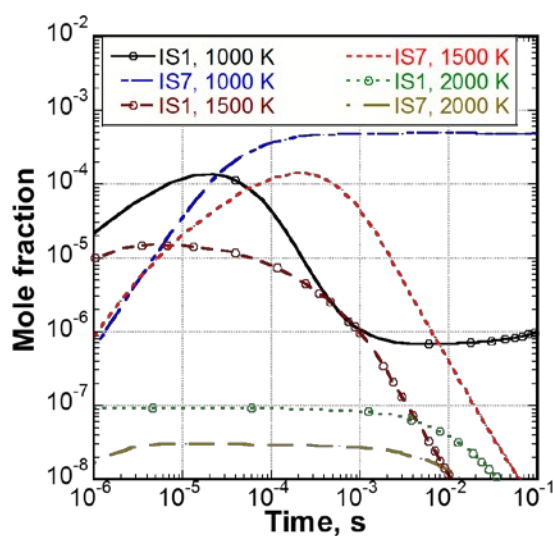
Figure 8: **(a)** Rate constants for $2benzyl \rightarrow bibenzyl$ ($IS1$). The terms “Exp(a)”, “Exp(b)” and “Exp(c)” in the legend represent experimental data from [48], [49], and [50], respectively. The rate constants from CBS-QB3 and B3LYP/6-311++G(d,p) calculations are provided. The rate constant used in [36] are also presented. **(b)** Rate constants for $IS1$ decomposition reactions calculated using CBS-QB3. “Exp” represents experimental data from [50] for $IS1 \rightarrow 2benzyl$. The rate constant for $IS1 \rightarrow 2benzyl$ used in [36] are provided.



(a) Profiles of benzyl and H.



(b) Profiles of phenanthrene and anthracene.



(c) Profiles of IS1 and IS 7.

Figure 9: Species mole fractions profiles at temperatures of 1000, 1500 and 2000 K for benzyl, H, phenanthrene, anthracene (IS17), IS1, and IS7 obtained through isothermal batch reactor simulations.

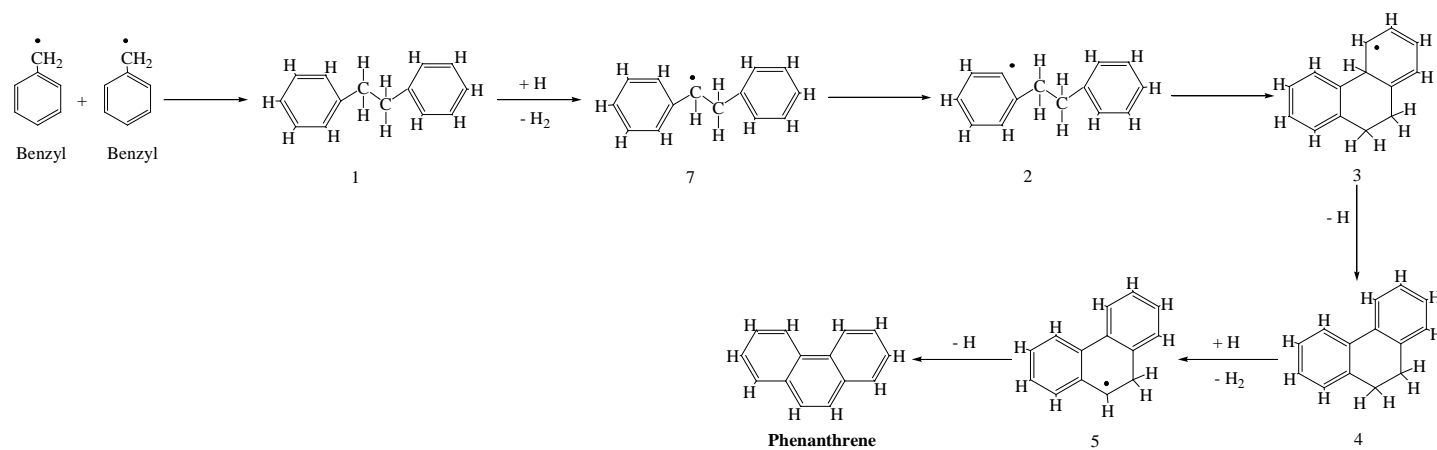
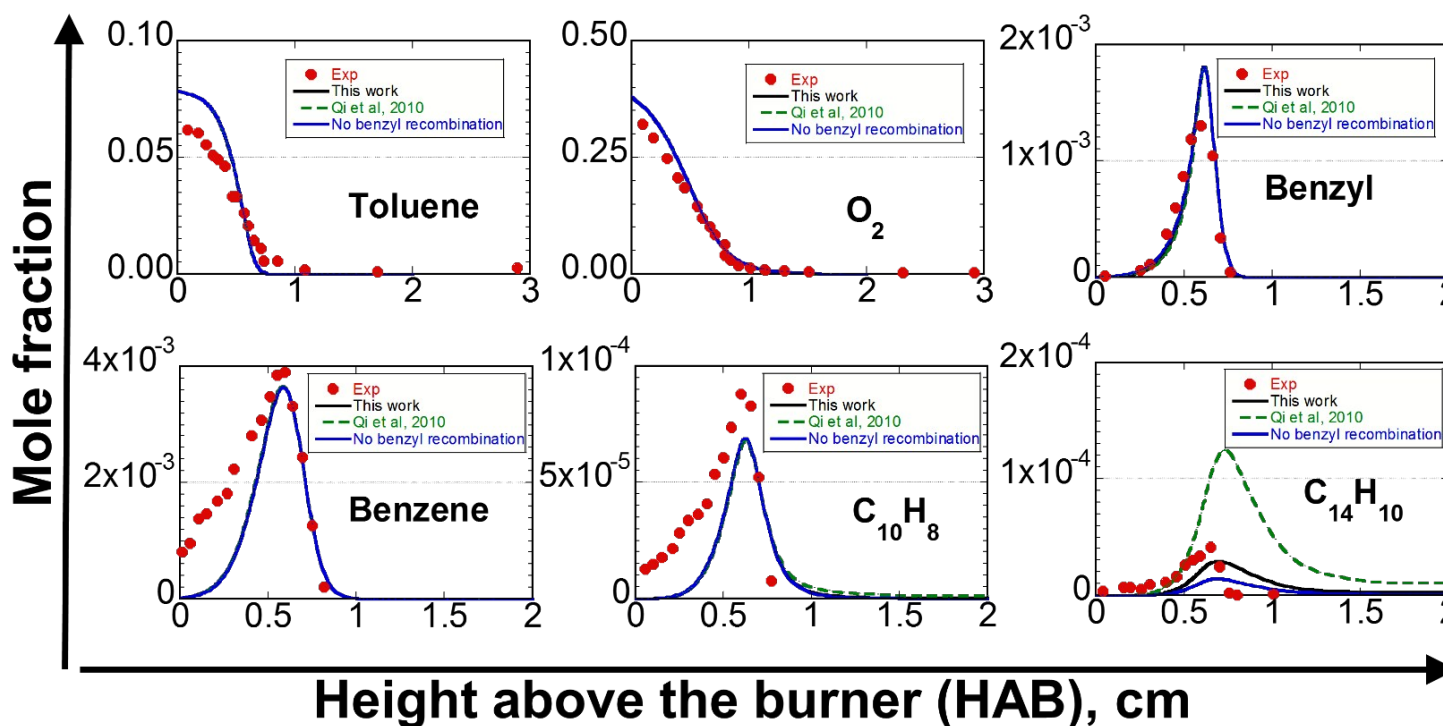
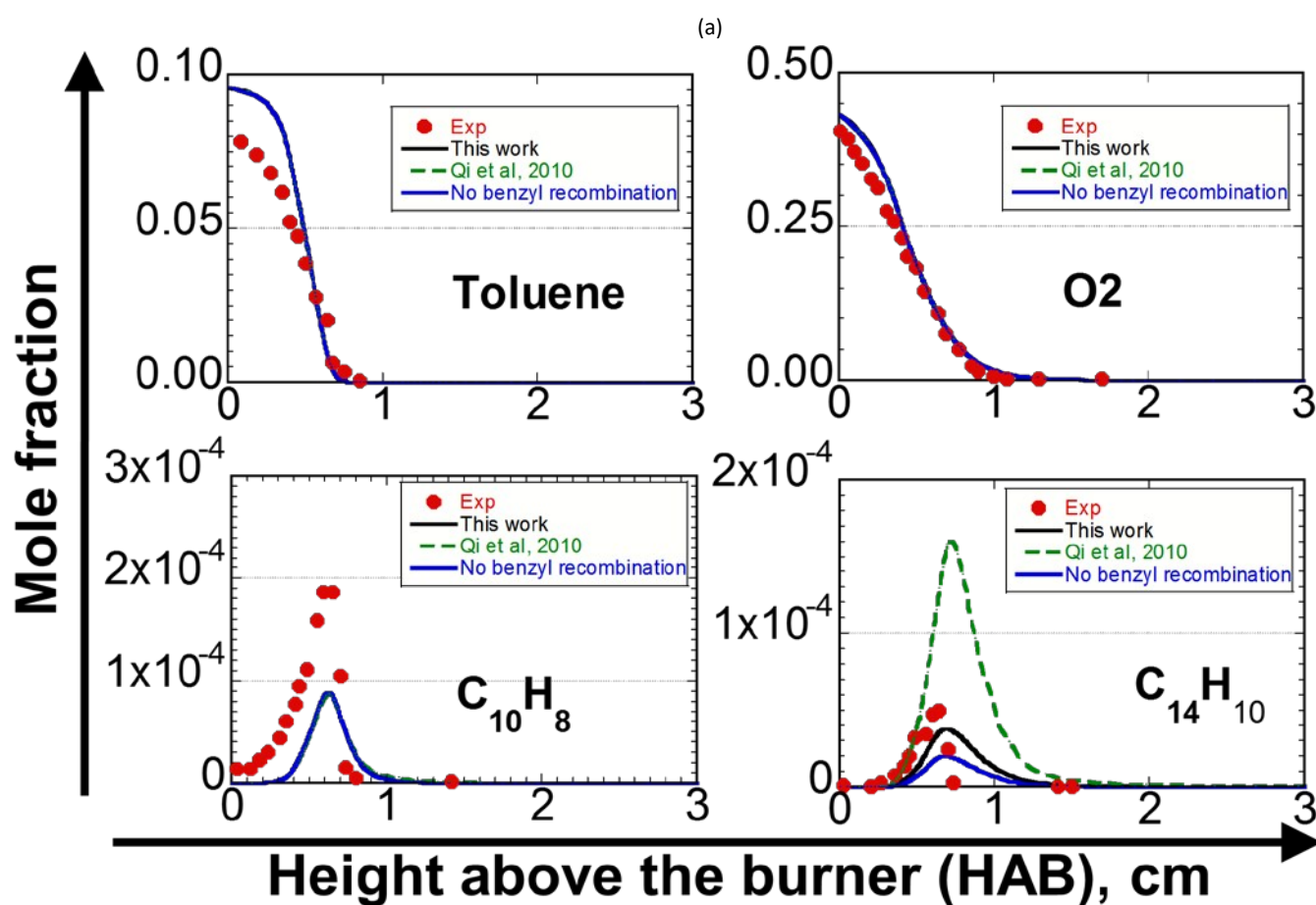


Figure 10: Main reactions involved in phenanthrene formation from benzyl radicals.



Height above the burner (HAB), cm



(b)

Figure 11: Experimental and simulated profiles of chemical intermediate species in two premixed laminar toluene flames. (a) Flame conditions: Mole fractions of toluene, O_2 and Ar are 0.0814, 0.4186 and 0.5, respectively, pressure is 4 kPa, and feed inlet velocity is 35 cm/s [54]. (b) Flame conditions: Mole fractions of toluene, O_2 and Ar are 0.0998, 0.4731 and 0.4271, respectively, pressure is 4 kPa, and feed inlet velocity is 31.5 cm/s [53]. The experimental temperature profiles are provided in the respective references.

